PEOPLE'S DEMOCRATIC REPUBLIC OF ALGERIA

MINISTRY OF HIGHER EDUCATION AND RESEARCH SCIENTIST

MOHAMED BOUDIAF UNIVERSITY - M'SILA

Faculty of technologie

Electrical Engineering Department


# MODELING AND CONTROL OF A GRID-CONNECTED PHOTOVOLTAIC SYSTEM

by

Aouachria Ali Abderrahmane

A Master's Thesis

Submitted in Partial Fulfillment of the Requirements

for the Degree of Professional Master

in RENEWABLE ENERGIES / GREEN HYDROGEN ENERGY VECTOR

[ 23 / 06 / 2025 ]

Jury members:

| | | |
|---|---|---|
| Advisor | Dr. BENTATA Khadidja | M'sila University |
| Co-Advisor | Pr. BENSLIMANE Tarak | M'sila University |
| President | Pr. BENYETTOU Lotfi | M'sila University |
| Examiner | Dr. BOUDJELLAL Bilal | M'sila University |

Academic year : 2024 / 2025

**Abstract**

The growing integration of photovoltaic (PV) power into the grid has brought on challenges related to grid stability, with the boost converter and the inverter introducing harmonics and instability, especially under non-linear loads and environmental changes. Therefore, conducting practical testing on grid-connected PV systems under various conditions can be difficult and often impossible due to the destructive nature of many scenarios. Existing research often lacks comprehensive modeling, realworld validation, and explicit adherence to grid connection standards. Thus, this thesis aims to present a detailed modeling, design, and control strategy for a grid-connected PV system that accurately reflects the behavior of the 100-kilowatt-peak (kWp) PV plant, while adhering to the IEEE 929–2000 and European EN 50160 grid connection standards. The developed one hundred-kilowatt model encompasses all components of the double-stage topology, namely the PV array, boost converter, maximum power point tracking (MPPT) controller, three-phase pulse width modulation (PWM), voltage source inverter (VSI), LC filter, grid synchronization technique with a phase-locked loop (PLL), VSI dual-loop current controller with PI regulators, and other grid connection components. The entire proposed model, implemented in MATLAB/Simulink, was used to simulate various scenarios under different weather conditions, including standard test conditions (STC), a sudden drop in solar irradiation, and a real-world scenario.

**Keywords :** Grid-connected PV system · MPPT controller · Three-Level NPC VSI · LC filter design · PLL · Double-stage topology.

ملخص :

أدى التكامل المتزايد للطاقة الكهروضوئية (PV) في الشبكة إلى ظهور تحديات تتعلق باستقرارها، حيث يُدخل مُحَوِّل التعزيز والعاكس التوافقيات ويُسببان عدم استقرار، خاصةً في ظل الأحمال غير الخطية والتغيرات البيئية. لذلك، قد يكون إجراء اختبارات عملية على أنظمة الطاقة الكهروضوئية المتصلة بالشبكة في ظل ظروف مُختلفة أمرًا صعبًا، بل مستحيلًا في كثير من الأحيان، نظرًا للطبيعة المُدمرة للعديد من السيناريوهات. غالبًا ما تفتقر الأبحاث الحالية إلى النمذجة الشاملة، والتحقق من الصحة في العالم الحقيقي، والالتزام الصريح بمعايير توصيل الشبكة. لذا، تهدف هذه الأطروحة إلى تقديم استراتيجية مُفصلة للنمذجة والتصميم والتحكم لنظام طاقة كهروضوئية متصل بالشبكة، تعكس بدقة سلوك محطة الطاقة الكهروضوئية ذات ذروة 100 كيلوواط (kWp) مع الالتزام بمعايير توصيل الشبكة (IEEE 929-2000) و(EU EN 50160) يشمل نموذج المائة كيلوواط المُطوَّر جميع مكونات طوبولوجيا المرحلتين، وهي: مصفوفة الخلايا الكهروضوئية، ومُحَوِّل التعزيز، ووحدة تحكم تتبع نقطة القدرة القصوى (MPPT)، وتعديل عرض النبضة ثلاثي الطور (PWM)، وعاكس مصدر الجهد (VSI)، ومرشح LC ، وتقنية مزامنة الشبكة باستخدام حلقة مغلقة الطور (PLL)، ووحدة تحكم تيار VSIثنائية الحلقة مع منظمات (PI)، ومكونات أخرى لتوصيل الشبكة. استُخدم النموذج المقترح بالكامل، والمُنفَّذ في (MATLAB/Simulink)، لمحاكاة سيناريوهات مُختلفة في ظل ظروف جوية مُختلفة، بما في ذلك ظروف الاختبار القياسية (STC)، والانخفاض المفاجئ في الإشعاع الشمسي، وسيناريو واقعي.

الكلمات المفتاحية: نظام كهروضوئي مُتصل بالشبكة · وحدة تحكم (MPPT)، ثلاثي المستويات (NPC VSI)، تصميم مرشح (PLL)، (LC)، طوبولوجيا المرحلتين.

**Acknowledgements**

*I would like to express my deepest gratitude to my family, colleagues and teachers for their unwavering support and encouragement throughout the course of this research. Their contributions, whether through intellectual insight, emotional support, or practical assistance, have been invaluable in helping me complete this thesis. I am especially grateful to supervisor, whose expert guidance, patience, and mentorship have been instrumental in shaping this project. Their insightful feedback and constructive criticism pushed me to refine my ideas and helped elevate the quality of this work.*

*I would also like to extend my heartfelt thanks to researchers of researchgate academic platform, whose resources and support were crucial in enabling me to conduct this research. Without their generosity and assistance, this project would not have been possible.*

*A special thank you goes to my family and friends for their constant encouragement, understanding, and patience. Their support helped me stay focused during the most challenging moments of this journey. your belief in me gave me the strength to persevere.*

## Table of Contents

## List of Tables

## List of Figures

## Chapter I : Introduction

### *I. 1* ***Background :***

Increasing environmental concerns regarding the inefficient use of energy, climate change, acid rain, stratospheric ozone depletion, and global dependence on electricity have directed attention to the importance of generating electric power in a sustainable manner with low emissions of GHGs, particularly $CO_2$. To achieve this, many industrialized countries seek to decarbonize electricity generation by replacing conventional coal and fossil fuel fired plants with renewable technology alternatives [1].

Due to the shortage of inexhaustible resources and environmental problems caused by the emissions, the traditional power generations, which are based on fossil fuel are generally considered to be unsustainable in the long term. As a result, many efforts are made worldwide and lots of countries have being introducing more renewable energies, such as wind power, solar photovoltaic (PV) power, hydropower, biomass power, and ocean power, etc. into their electric grids [2]. Currently, a significant portion of electricity is generated from fossil fuels, especially coal due to its low prices. However, the increasing use of fossil fuels accounts for a large amount of environmental pollution and GHG emissions, which are considered the main reason behind the global warming. For example, the emissions of carbon dioxide and mercury are expected to increase by 35 % and 8 %, respectively, by the year 2020 due to the expected increase in electricity generation. Furthermore, possible depletion of fossil fuel reserves and unstable price of oil are two main concerns for industrialized countries [3]. While the prices for fossil fuels are skyrocketing and the public acceptance of these sources of energy is declining, PV technology has become a truly sensible alternative. Solar energy plays a major role since it is globally available, flexible

with regard to the system size and because it can fulfill the needs of different countries since it offers on-grid and off-grid solutions [4]. The boundless supply of sunlight and wind and their zero emission power generation become a driving force in the fast growth of PV and Wind systems technology. Unlike the dynamic wind turbine, PV installation is static, does not need strong high towers, produces no vibration, and does not need cooling systems. In addition, it is environmentally friendly, safe, and has no gas emissions [4]. The use of PV systems in electricity generation started in the seventies of the twentieth century and today is currently growing rapidly around worldwide in spite of high capital cost [3]. PV systems convert the sun's energy directly into electricity using semiconductor materials. They differ in complexity, some are called "stand-alone or off-grid" PV systems, which signifies they are the sole source of power to supply building loads. Further complicating the design of PV systems is the possibility to connect the PV system generation to the utility "grid connected or on-grid" PV systems, where electrical power can either be drawn from grid to supplement system loads when insufficient power is generated or can be sold back to the utility company when an energy surplus is generated [5][6]. Based on prior arguments, grid-connected, or utility-interactive systems appear to be the most practical application for buildings where the available surface is both scarce and expensive. Grid-connected PV systems currently dominate the PV market, especially in Europe, Japan, and USA. With utility interactive systems, the public electricity grid acts as an energy store, supplying electricity when the PV system cannot. The performance of a PV system largely depends on solar radiation, temperature and conversion efficiency. Although, PV systems have many advantages, they suffered from changing of system performance due to weather variations, high installation cost, and low efficiency that is hardly up to 20 % for module [7]. An interesting problem associated with PV systems is the optimal computation of their size. The sizing optimization of stand-alone

or grid connected PV systems is a convoluted optimization problem which anticipates to obtain acceptable energy and economic cost for the consumer [8].

*I. 2* ***Problem Statement :***

In modern power systems, the rapid expansion of photovoltaic (PV) generation presents both opportunities and challenges for grid operators. While large-scale, grid-connected PV plants offer clean energy and reduced reliance on fossil fuels, their intermittent output and nonlinear dynamic behavior can compromise voltage stability, power-quality, and overall system reliability. Traditional modeling approaches often oversimplify the PV array's electrical characteristics or the grid's dynamic response, leading to inaccurate predictions under transient conditions (e.g., cloud-cover events, grid faults, or sudden load changes).

My thesis will address the following core problem: **How can a high-fidelity, Simulink model of a 100 kW grid-connected PV system be developed and validated to accurately capture both steady-state performance and dynamic interactions with the utility grid, thereby enabling more reliable stability and control studies?**

Key elements of the problem statement include:

1. **Modeling accuracy gap**: Existing Simulink blocks (e.g., built–in PV Array, Inverter, and PQ Controller) lack customization for site-specific irradiance, temperature profiles, and grid-impedance characteristics, limiting their validity for precise case-study analysis.

2. **Dynamic behavior under disturbances**: There is insufficient representation of how grid disturbances—such as voltage sags/swells or frequency deviations—propagate through power-electronic interfaces and affect the PV output and stability margins.

3. **Control strategy evaluation**: Without a detailed model, it is difficult to test advanced inverter control schemes (e.g., virtual synchronous generator or enhanced reactive-power dispatch)

in a realistic environment. By constructing a comprehensive, state-space model in MATLAB/Simulink—parameterized with real-world data—your research will:

* Validate the model against measured plant data under varying irradiance and temperature.

* Simulate grid-disturbance scenarios to assess voltage stability and power-quality impacts.

* Provide a test-bed for evaluating and optimizing inverter control algorithms.

The outcome will bridge the gap between simplified PV models and the complex realities of grid integration, supporting more robust design and operational strategies for large-scale PV plants.

### *I. 3* ***Objectives and Aims :***

Develop a High-Fidelity Simulation Platform: Create a comprehensive MATLAB/Simulink environment that accurately represents a 100 kW grid-connected PV system—covering PV array behavior, DC–DC conversion, inverter dynamics, and grid interaction.

Bridge Modeling Gaps: Address limitations in standard Simulink PV/inverter blocks by embedding site-specific irradiance, temperature, and grid-impedance data for the plant.

Enable Advanced Control Studies: Provide a flexible test-bed for evaluating both conventional and cutting-edge inverter control strategies (e.g., PI-based PQ control, virtual synchronous generator emulation, enhanced reactive-power dispatch).

Enhance Grid-Integration Insights: Use the model to investigate how large-scale PV plants affect voltage stability, power quality, and fault-ride-through performance under realistic disturbance scenarios.

### *I. 4* ***Thesis Structure :***

This thesis is structured as follows: Chapter 1 provides an introduction to the research. Chapter 2 reviews the relevant literature. Chapter 3 details the methodology used in the study. Chapter 4 presents the findings, and Chapter 5 discusses the implications and conclusions.

# Chapter II : Literature Review

## *II. 1 Photovoltaic Systems Overview :*

Photovoltaic systems can be grouped into stand-alone systems and grid-connected systems as illustrated in Fig. 1.3. In stand-alone systems the solar energy yield is matched to the energy demand. Since the solar energy yield often does not coincide in time with the energy demand from the connected loads, additional storage systems (batteries) are generally used. If the PV system is supported by an additional power source, for example, a wind or diesel generator this is known as a PV hybrid system. In grid-connected systems the public electricity grid functions as an energy

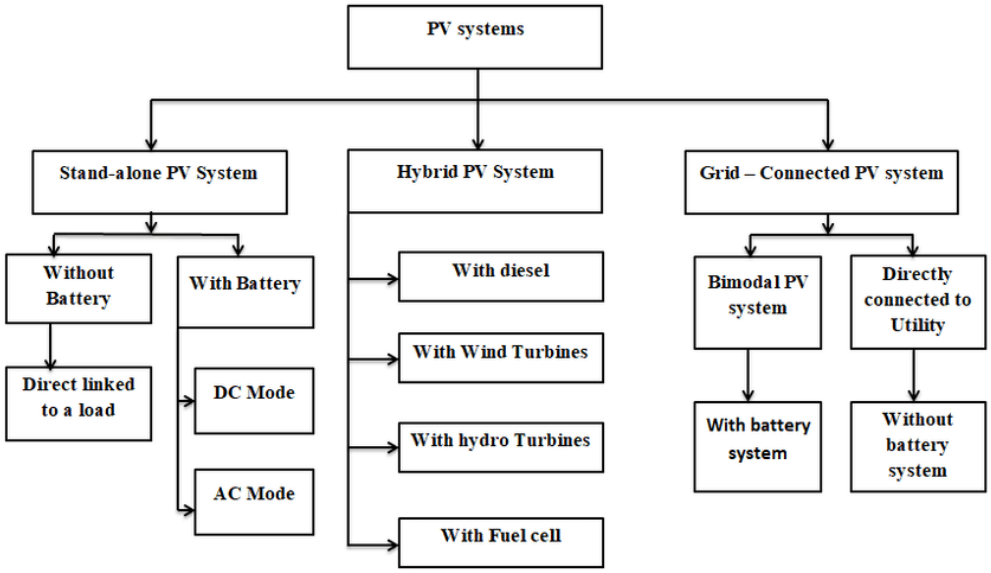


*Figure 1: PV systems classifications.*

store [9] .

### *II . 1 . 1 Stand-alone Systems :*

The first cost-effective applications for photovoltaics were stand-alone systems. Wherever it was not possible to install an electricity supply from the mains utility grid (UG). The range of applications is constantly growing. There is great potential for using stand-alone systems in

developing countries where vast areas are still frequently not supplied by an electrical grid. These systems can be seen as a well-established and reliable economic source of electricity in rural areas, especially where the grid power supply is not fully extended [10]. Solar power is also on the advance when it comes to mini-applications: pocket calculators, clocks, battery chargers, flashlights, solar radios, etc., are well-known examples of the successful use of solar cells in stand-alone applications.

Stand-alone PV systems generally require an energy storage system because the energy generated is not usually required at the same time as it is generated (i.e., solar energy is available during the day, but the lights in a stand-alone solar lighting system are used at night). Rechargeable batteries are used to store the electricity. However, with batteries, in order to protect them and achieve higher availability and a longer service life it is essential that a suitable charge controller is also used as a power management unit. Hence, a typical stand-alone system comprises the following main components [11]:

1. PV modules, usually connected in parallel or series-parallel;
2. Charge controller;
3. Battery or battery bank;
4. Loads;
5. Inverter (i.e., in systems providing AC power).

#### *II . 1 . 2 Grid-Connected Photovoltaic Systems :*

The basic building blocks of a grid-connected PV system are shown in Fig. 2. The system is mainly composed of a matrix of PV arrays, which converts the sunlight to DC power, and a power conditioning unit (PCU) that converts the DC power to an AC power. The generated AC power is injected into the UG and/or utilized by the local loads. In some cases, storage devices are used to

improve the availability of the power generated by the PV system. In the following subsections, more details about different components of the PV system are presented. A grid connected PV system eliminates the need for a battery storage bank resulting in considerable reduction of the initial cost and maintenance cost. The PV system, instead, uses grid as a bankwhere the excess electric power can be deposited to and when necessary also withdrawn from.

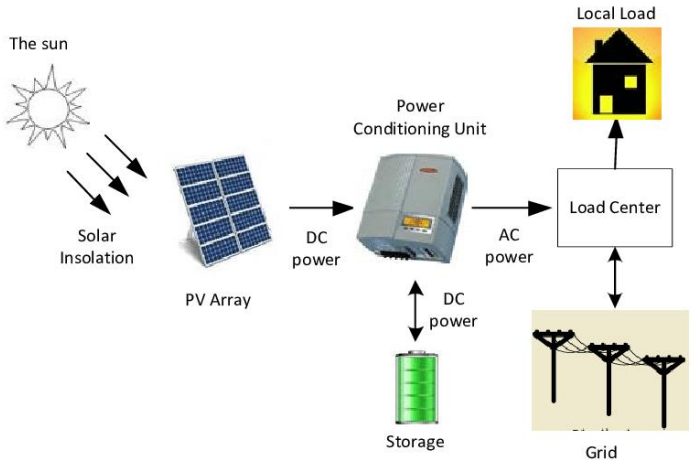


*Figure 2: Main components of grid-connected PV systems.*

### *II . 1 .2 .1 The Photovoltaic Cell/Module/Array :*

The PV cell is the smallest constituent in a PV system. A PV cell is a specially designed P-N junction, mainly silicon-based semiconductor and the power input is made possible by a phenomenon called the photoelectric effect. The characteristic of photoelectric effect was discovered by the French scientist, Edmund Bequerel, in 1839, when he showed that some materials produce electricity when exposed to sunlight. The photons in the light are absorbed by the material and electrons are released, which again creates a current and an electric field because of charge transfer. The nature of light and the photoelectric effect has been examined by several

scientists the last century, for instance Albert Einstein, which has led to the development of the solar cell as it is today [12].

In most practical situations the output from a single PV cell is smaller than the desired output. To get the adequate output voltage, the cells are connected in series into a PV module. When making a module, there are a couple of things that need to be considered.

• No or partly illumination of the module: During the night, when none of the modules are illuminated, an energy storage (like a battery) connected directly in series with the modules makes the cells forward biased. This might lead to a discharge of the energy storage. To prevent this from happening a blocking diode can be connected in series with the module. But during normal illumination level this diode represents a significant power loss.

• Shading of individual cells: If any of the cells in a module is shaded, this particular cell might be forward biased if other unshaded parts are connected in parallel. This can lead to heating of the shaded cell and premature failure. To protect the system against this kind of failure, the modules contain bypass diodes which will bypass any current that cannot pass through any of the cells in the module.

If the output voltage and current from a single module is smaller than desired, the modules can be connected into arrays. The connection method depends on which variable that needs to be increased. For a higher output voltage the modules must be connected in series, while connecting them in parallel in turn gives higher currents. It is important to know the rating of each module when creating an array. The highest efficiency of the system is achieved when the MPP of each of the modules occurs at the same voltage level. Figure 3 shows the relation between the PV cell, a module and an array.

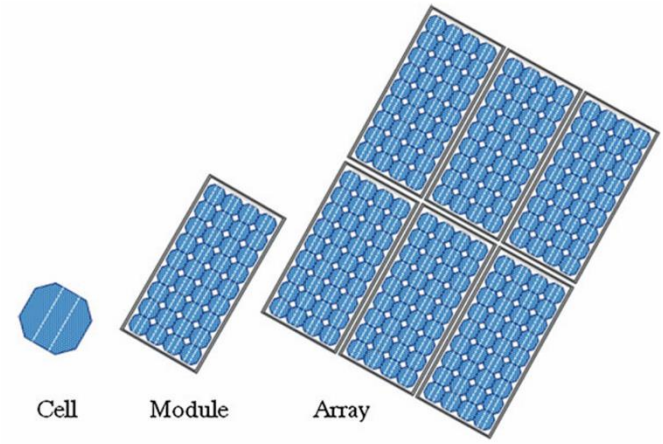


*Figure 3 : Relation between the PV cell, a module and an array.*

### *II . 1 . 3 Power Conditioning Units :*

Power conditioning units are used to control the DC power produced from the PV arrays and to convert this power to high-quality AC power before injecting it into the UG. PV systems are categorized based on the number of power stages. The past technology used single-stage centralized inverter configurations. The present and future technology focus predominantly on the two-stage inverters, where a DC–DC converter is connected in between the PV modules and the DC–AC inverter as shown in Fig. 4.

In single-stage systems, an inverter is used to perform all the required control tasks. But, in the two-stage system, a DC–DC converter precedes the inverter and the control tasks are divided among the two converters. Two-stage systems provide higher flexibility in control as compared to single-stage systems, but at the expense of additional cost and reduction in the reliability of the system [13]. During the last decade, a large number of inverter and DC–DC converter topologies for PV systems were proposed [13] [14], In general, PCUs have to perform the following tasks:

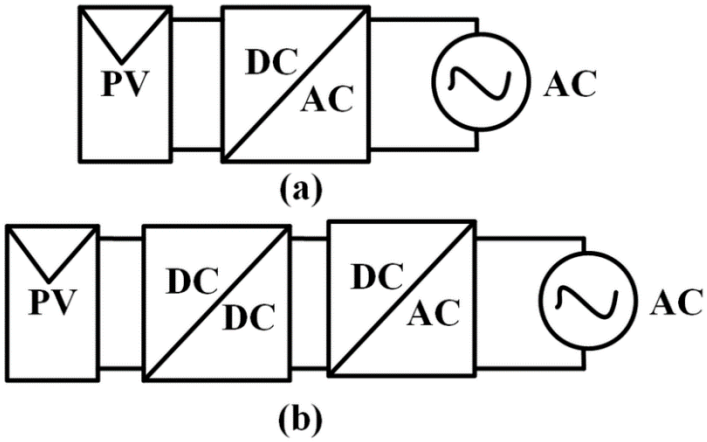


*Figure 4: Classification of system configurations (a) single stage (b) two stages.*

## *II. 2 Theoretical Framework :*

### *II . 2 . 1 Photovoltaic Generator (PVG) model :*

Although PV systems have many advantages, they suffered from changing of system performance due to weather variations (solar radiation, temperature), high installation cost, and low efficiency that is hardly up to 20 % for module. Therefore, the modeling of PV system is an important aspect to describe performance of the PV systems. Kim et al. [15] present a mathematical model describing PV module behavior individually and in a series/parallel as connected in a PV system. Figure 5 shows a PV array, which consists of multiple modules, linked in series and parallel manners. The number of modules modifies the value of series and parallel resistances. The value of equivalent series and parallel resistances of the PV system are given as :

$$R_{s,\text{array}} = \frac{N_s}{N_p} \cdot R_s \quad (1)$$

$$R_{s,\text{array}} = \frac{N_p}{N_s} \cdot R_s \quad (2)$$

$$I_a = N_p I_{ph} - N_p I_o \left[ \exp\left( \frac{q}{AKT} \left( \frac{V_a}{N_s} + \frac{I_a R_s}{N_p} \right) \right) - 1 \right] - \frac{1}{R_{sh}} \left( \frac{V_a}{N_s} + \frac{I_a R_s}{N_p} \right) \quad (3)$$

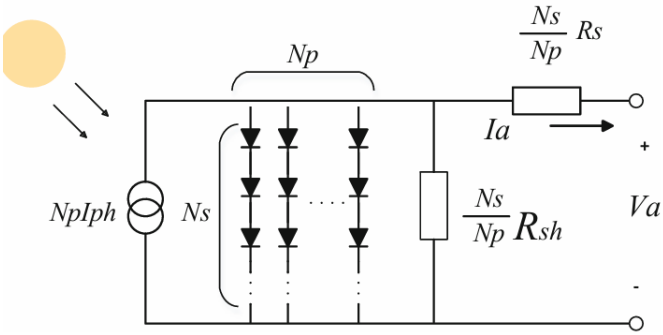


*Figure 5: Equivalent circuit of PV array.*

### *II . 2 .1 .1 Calculation of Optimal Number of PV Modules :*

The number of subsystems, $N_{sub}$ depends on the inverter rating, $P_{inverter}$ and size of PV system, $P_{system}$ : $N_{sub} = \frac{P_{system}}{P_{inverter}}$ (4)

Series and parallel combination of each PV subsystem can be adjusted according to not only the MPP voltage range but also maximum DC input current of the inverter. Estimation of the initial total number of PV modules for each subsystem can be calculated as follows:

$$N_{PV\_sub\_i} = \frac{P_{inverter}}{P_{max}} \quad (5)$$

Most manufacturers of inverters for PV systems make a wide range between the maximum and minimum values of MPP voltage range ($V_{mpp\_max}$;$V_{mpp\_min}$), where inverters act properly and have no problem to find the maximum power point in where the module is working. Minimum and the maximum number of PV modules that can be connected in series in each branch, $N_{s\_min}$ and $N_{s\_max}$, respectively, are calculated according to the MPP voltage range as follows:

$$N_{s\_min} = \left\lceil \frac{V_{mpp\_min}}{V_{mpp}} \right\rceil \quad (6)$$

$$N_{s\_\max} = \left\lceil \frac{V_{mpp\_\max}}{V_{mpp}} \right\rceil \qquad (7)$$

where $V_{mpp}$ is the maximum power point of PV module. The optimal number of series modules, $N_{s\_sub}$ is located in the range of : $N_{s\_min} < N_{s\_sub} < N_{s\_max}$

Minimum and the maximum number of PV modules that can be connected in parallel in each subsystem, $N_{p\_min}$ and $N_{p\_max}$, respectively, are calculated as follows:

$$N_{\mathrm{p\_min}} = ceil\left(\frac{N_{\mathrm{pv\_sub\_i}}}{N_{\mathrm{s\_max}}}\right) \qquad (8)$$

$$N_{p_{max}} = ceil\left(\frac{N_{PV\_sub_i}}{N_{s_{min}}}\right) \qquad (9)$$

where optimal number of parallel modules $N_{p\_sub}$ is located in the range of :

$$N_{\mathrm{p_{min}}} < N_{\mathrm{p_{sub}}} < N_{\mathrm{p_{max}}}$$

Number of PV modules connected in parallel $N_{p\ sub}$ may be set to $N_{p\ min}$ but cannot be set to $N_{p\ max}$, because the DC current results from all parallel strings may be higher than the maximum DC input of the inverter which may damage the inverter. For each number of series modules, $N_{s\ sub}$ in the series range calculated previously, estimation of the corresponding parallel modules for each subsystem can be calculated as follows:

$$N_{\mathrm{p_{sub}}} = ceil\left(\frac{N_{\mathrm{PV_{subi}}}}{N_{\mathrm{s_{sub}}}}\right) \qquad (10)$$

Then, recalculate the total number of PV module, $N_{PV\ sub}$ according to each resulted series and parallel combination : $N_{\mathrm{PV\ sub}} = N_{\mathrm{s\ sub}} \cdot N_{\mathrm{p\ sub}}$ (11)

Assuming that inverter is operating in the MPP voltage range, the operating input voltage and current of the inverter ( $V_{mpp\ sub}$; $I_{mpp\ sub}$ ) can be calculated as follows:

$$V_{\mathrm{mpp\_sub}} = N_{s\_sub} \cdot V_{\mathrm{mpp}} \qquad (12)$$

$$I_{\text{mpp\_sub}} = N_{p\_sub} \cdot I_{\text{mpp}} \qquad (13)$$

From previous calculations, a database containing probable series and parallel combinations, PV modules, DC input voltage and current for each subsystem is formed. Optimal total number of PV modules for each subsystem is selected according to minimum number of PV modules which satisfies not only the MPP voltage range but also the maximum DC input current of the inverter. The total number of PV modules, $N_{PV}$ for the selected site can be calculated from the following:

$$N_{\text{PV}} = N_{\text{sub}} \cdot N_{\text{PV}_{\text{sub}}} \qquad (14)$$

### *II . 2 . 2 Modeling of DC–DC Boost Converter :*

Photovoltaic modules have a low efficiency compared to some other RESs. In such systems the input is often fluctuating due to variation of solar radiation and the output is required to be constant. As a consequence, it is mandatory to adopt an intermediate conversion stage, interfacing the PV system with the inverter and maximizing the power output from PV array through an MPPT algorithm. This can be done through a DC–DC boost converter. The converter can operate in two different modes of operation depending on its energy storage capacity and the relative length of the switching period. These two operating modes are known as CCM and discontinuous conduction mode.

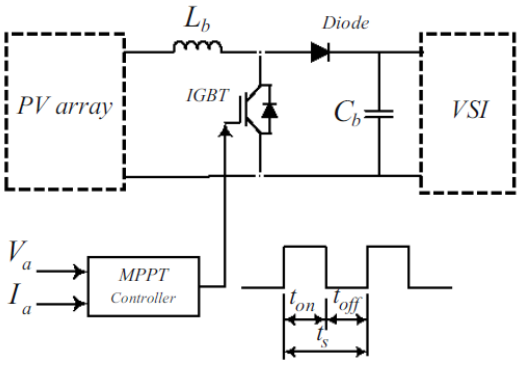


*Figure 6: DC–DC boost converter and its controller.*

converter configuration and its controller. The output voltage of the boost converter during CCM is given by [16] : $V_{\mathrm{DC}} = \frac{V_{\mathrm{PV}}}{1-D}$ (15)

### *II . 2 .2 .1 MPPT Control System :*

Various MPPT methods are presented in literature [17]. Among all the MPPT methods, Perturb & Observe (P&O) and Incremental Conductance (IC) techniques are the most commonly used because of their simple implementation and faster time to track the MPP. All these algorithms have the advantage of being independent of the knowledge of the PV generator characteristics, so that the MPP is tracked regardless of the irradiance level, temperature, and degradation, thus ensuring high robustness and reliability [18]. The MPPT controller in the proposed system uses the IC technique.

### ***II . 2 . 3 Modeling of Voltage Source Inverter :***

To convert the DC link voltage into AC voltage for supplying the AC load or to inject active/reactive power into the UG, a DC–AC power conversion is carried out using the grid-interfacing VSI.

*II . 2 .3 .1 Traditional Two-Level Voltage Source Inverter :*

The 2L-VSI topology has been widely used for a range of power levels since 1990s due to its fast switching characteristic performance. The schematic diagram of this topology is shown in Fig. 7. There are two switches per phase. It is capable of producing two output voltage levels namely + $V_{dc}$ and -$V_{dc}$.

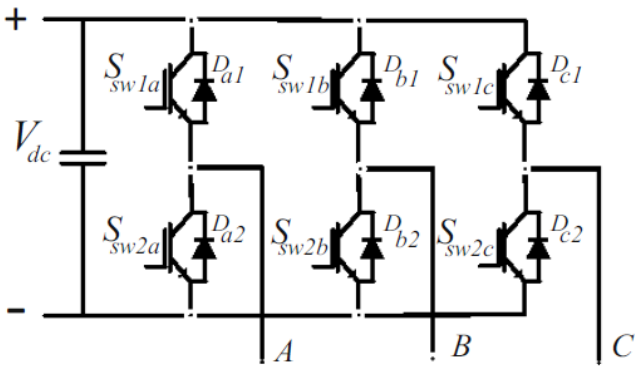


*Figure 7 : The power circuit diagram of a three-phase 2L-VSI.*

The thumb rule in control theory of the operating switching frequency range for 2L-VSI must be 10 times higher than the resonant frequency of the LC filter, which is proven by Steinke[19] . A reduction of filter requirement with high resonant frequency is done by selecting very high switching frequency. However, 2L-VSI with high switching frequency may cause high dv/dt across power semiconductor devices. Under such condition, the switching device may experience high voltage spike which is higher than the DC link voltage. Hence, a device with higher voltage rating must be selected. Devices with such high voltage rating incur an additional switching loss due to additional stray losses occurring during the switching transition [20].

So more number of switches need to be added in series. Simultaneous switching of a series chain of IGBT’s becomes complex, as there may occur a delayed switching owing to heating of the devices. Hence, the concept of MLIs was introduced. It gave flexibility in switching the devices independently and at lower frequencies. Different topologies have been developed and a lot of

research is being done in improving the overall performance of the converter to provide an output of high quality.

### *II . 2 .3 .2 Multilevel Inverter Using Diode or Neutral-Point-Clamped Topology :*

The 3L-NPCVSI topology is one of the most commercialized MLI topologies on the market. In an MLI using diode-clamped topology, proposed by Nabae et al. [21], the single DC bus voltage is divided into a number of sublevels. The switching devices are connected in series and diodes are required to provide a connection to the subvoltage levels. The simplified schematic of 3L-NPCVSI is shown in Fig. 8. The middle point of the DC link (between two capacitors) is called the neutral point (N) and it is common for all three phases. The voltage division is reached with the help of the diodes connected to the neutral point and that is also why this topology is very often called diode-clamped topology. For a 3L-NPCVSI, each phase consists of four switches and two diodes. The DC bus voltage is divided into three levels by means of two bulk capacitors ($C_1$ and $C_2$) connected in series. The output voltage has three states + Vdc ; 0; - Vdc. In each leg, there are two pairs of complementary switches ($S_1$ and $S_2$) and ($S_3$ and $S_4$) and two clamping diodes ($D_5$ and $D_6$). The outer switches ($S_1$ and $S_4$) are mainly operating for PWM and the inner switches ($S_2$ and $S_3$) are clamping the output terminal to the neutral point “N”. Table 1 lists the output voltage levels possible for one phase of the inverter. State condition 1 means the switch is ON, and 0 means the switch is OFF. The complementary switch pairs for phase leg “A” are ($S_{a1}$, $S_{a3}$), and ($S_{a2}$, $S_{a4}$).

From Table 1, it is observed that in a 3L-NPC VSI, the switches that are ON for a particular phase leg are always adjacent and in series.

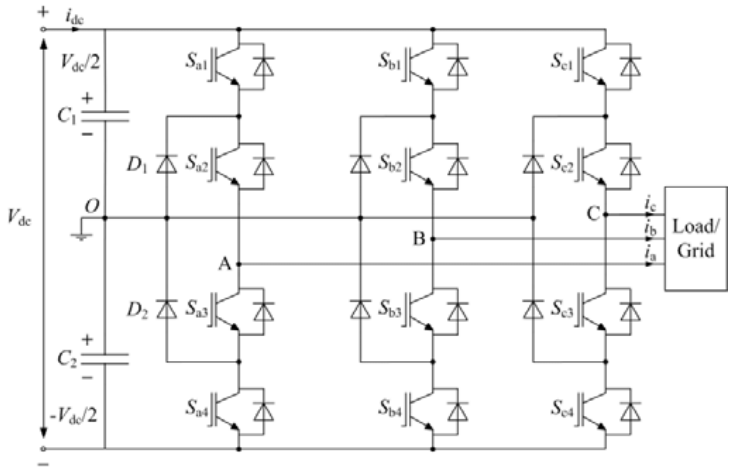


*Figure 8: The simplified schematic of 3L-NPCVSI .*

| Pole voltage, Va0 | Sa1 | Sa2 | Sa3 | Sa4 |
|---|---|---|---|---|
| Vdc/2 | 1 | 1 | 0 | 0 |
| 0 | 0 | 1 | 1 | 0 |
| -Vdc/2 | 0 | 0 | 1 | 1 |

*Table 1 : Voltage levels and corresponding switch states for a 3L-NPCVSI.*

### *II . 2 .3 .3 Control Theory of Voltage Source Inverters :*

Several modulation and control techniques have been developed for MLIs. As shown in Fig. 9, control techniques for MLIs can be classified into PWM, Selective Harmonic Elimination PWM (SHEPWM), and Optimized Harmonics Stepped PWM (OHSPWM) [22]. The regular PWM method can be classified as open loop and closed loop owing to its control strategy. The open-loop PWM techniques are SPMW, SVPWM, sigma–delta modulation, while closed-loop current control methods are defined as hysteresis, linear, and optimized current control techniques. The modulation methods developed to control the MLIs are based on multi-carrier orders with PWM. As predefined calculations are required, SHEPWM is not an appropriate solution for closed-loop

implementation and dynamic operation in MLIs. Among various control schemes, the sinusoidal PWM (SPWM) is the most commonly used control scheme for the control of MLIs. In SPWM, a sinusoidal reference waveform is compared with a triangular carrier waveform to generate switching sequences for power semiconductor in inverter module.

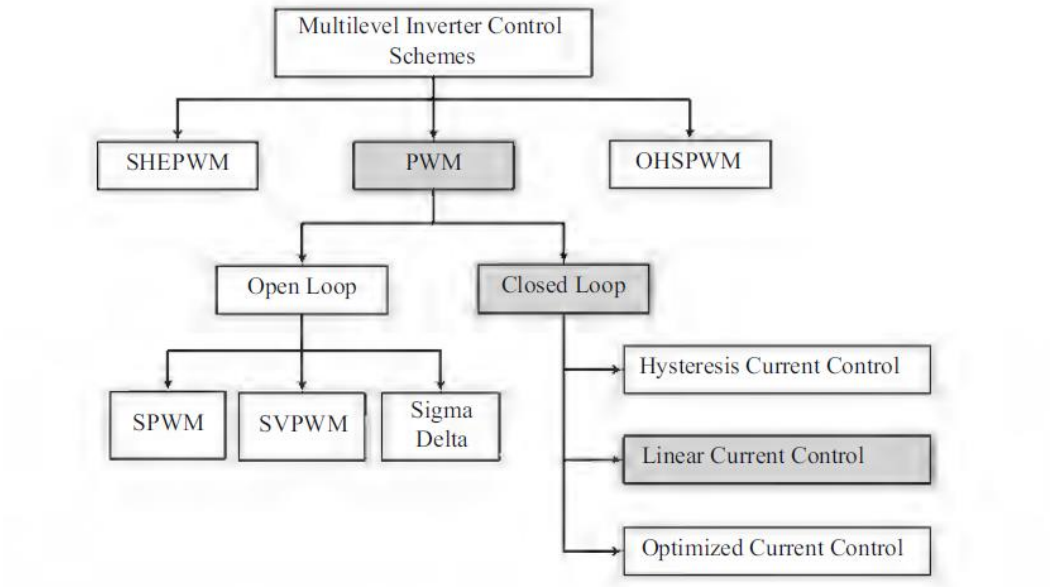


*Figure 9: Control schemes of MLIs .*

# Chapter III : Methodology

## *III. 1* ***Research Design :***

### *III . 1 . 1 System description :*

Multiple solar PV projects have already been completed as part of Algeria's national initiative for renewable energy, and more projects are in progress [23]. Nowadays, a total of twenty-one solar power plants with 344.1 MW capacities are installed in different cities in Algeria.

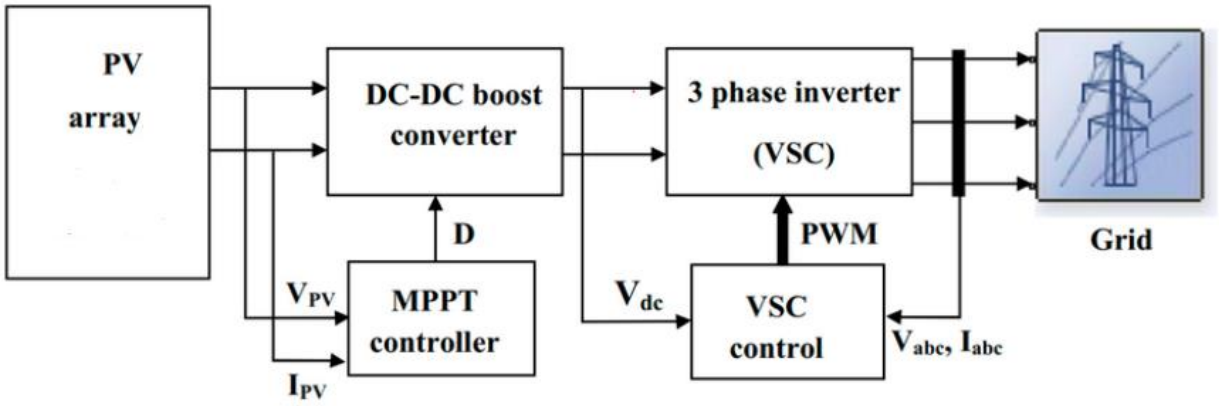


*Figure 10 : Structure of the studied grid-connected PV system.*

the double-stage configuration is adopted.

## ***III. 2 Modeling and control of DC stage :***

### *III . 2 . 1 Modeling of 100 kW PV array :*

A PV system is made up of a group of solar cells connected in both parallel and series to form an array. Based on meteorological information, such as temperature and irradiation levels, the single diode model (SDM) parameters ($I_{PV}$, $I_0$, $R_s$, and $R_p$) may be determined and modeled in Simulink by using the following mathematical equations.

The characteristic equation of PV module is :

$$I = I_{PV} - I_0 \left[\exp\left(\frac{q(V+IR_s)}{akTN_s}\right) - 1\right] - \frac{V+IR_s}{R_p} \qquad (1)$$

whereas for PV array Eq. (1) become:

$$I = I_{PV}.N_{pp} - I_0 \cdot N_{pp}\left[\exp\left(\frac{V+I\cdot R_S\left(\frac{N_{ss}}{N_{pp}}\right)}{a\cdot V_t\cdot N_{ss}}\right) - 1\right] - \frac{V+I\cdot R_s\cdot\left(\frac{N_{ss}}{N_{pp}}\right)}{R_p\cdot\left(\frac{N_{ss}}{N_{pp}}\right)} \qquad (2)$$

$$I_0 = \frac{I_{sc,n}+K_i\cdot\Delta T}{\exp\left(\frac{V_{oc,n}+K_v\cdot\Delta T}{a\cdot V_t}\right)-1} \qquad (3)$$

$$V_t = \frac{N_s\cdot k\cdot T}{q} \qquad (4)$$

$$I_{PV} = \left(I_{PV,n} + K_i\Delta T\right)\frac{G}{G_n} \qquad (5)$$

By using Eqs. (3) and (5), the model current $I_m$ of a PV array is produced.

$$I_m = I_{pv}\cdot N_{pp} - I_0\cdot N_{pp}\left[\exp\left(\frac{V+I\cdot R_s\left(\frac{N_{ss}}{N_{pp}}\right)}{a\cdot V_t\cdot N_{ss}}\right) - 1\right] \qquad (6)$$

*III . 2 .1 .1 Determination of series and parallel resistances :*

A Matlab program was devised to find $R_s$ and $R_p$ for the SunPower SPR-305E-WHT-D PV module used in the PV plant, using the iterative curve fitting method proposed in [24]. By increasing slowly Rs from zero while calculating the initial parallel resistance using Eq. (9) and ensuring that $P_{max,m}$ is equal to $P_{max,e}$ at the point ($V_{mpp}$, $I_{mpp}$) as seen in Fig. 11.

$$P_{max,m} = V_{mp}\left\{I_{pv} - I_0\left[\exp\cdot\left(\frac{q}{k\cdot T}\frac{V_{mp}+R_s\cdot I_{mp}}{a\cdot N_s}\right) - 1\right] - \frac{V_{mp}+R_s\cdot I_{mp}}{R_p}\right\} = P_{max,e} \qquad (7)$$

$$R_p = \frac{V_{mp}\cdot\left(V_{mp}+I_{mp}\cdot R_s\right)}{\left\{V_{mp}\cdot I_{pv} - V_{mp}\cdot I_0\cdot\exp\left[\frac{q}{k\cdot T}\frac{\left(V_{mp}+R_s\cdot I_{mp}\right)}{a\cdot N_s}\right] + V_{mp}\cdot I_0 - P_{max,e}\right\}} \qquad (8)$$

$$R_{p,min} = \frac{V_{mp}}{I_{sc,n} - I_{mp}} - \frac{V_{oc,n} - V_{mp}}{I_{mp}} \qquad (9)$$

By solving Eq. (1) with Newton–Raphson method, giving the current I as a function of V, and at each iteration the $I_{pv,n}$ is evaluated by:

$$I_{pv,n} = \frac{(R_p + R_s)}{R_p} I_{sc,n} \qquad (10)$$

the data of the manufacturer in Table 2 [25], and the obtained values of Rs and Rp in Table 3. The one-megawatt PV array used in this work is composed of $N_{ss}$ = 5 modules in each string and $N_{pp}$ = 66 strings in parallel. The I-V and P-V characteristics of this PV array are shown in Fig. 12.

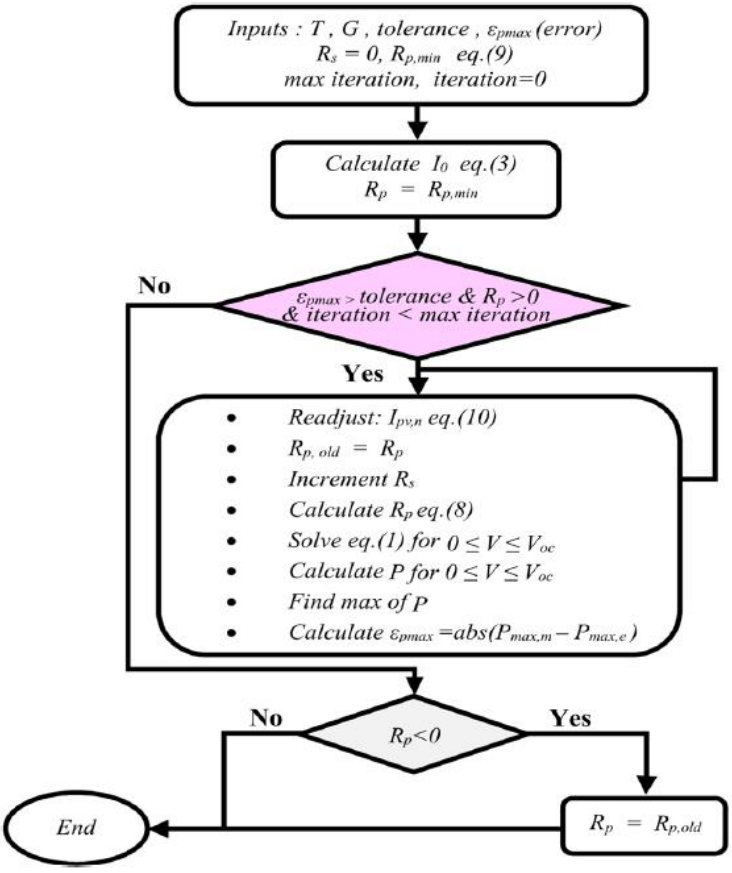


*Figure 11: Algorithm for determining RS and RP of PV panel.*

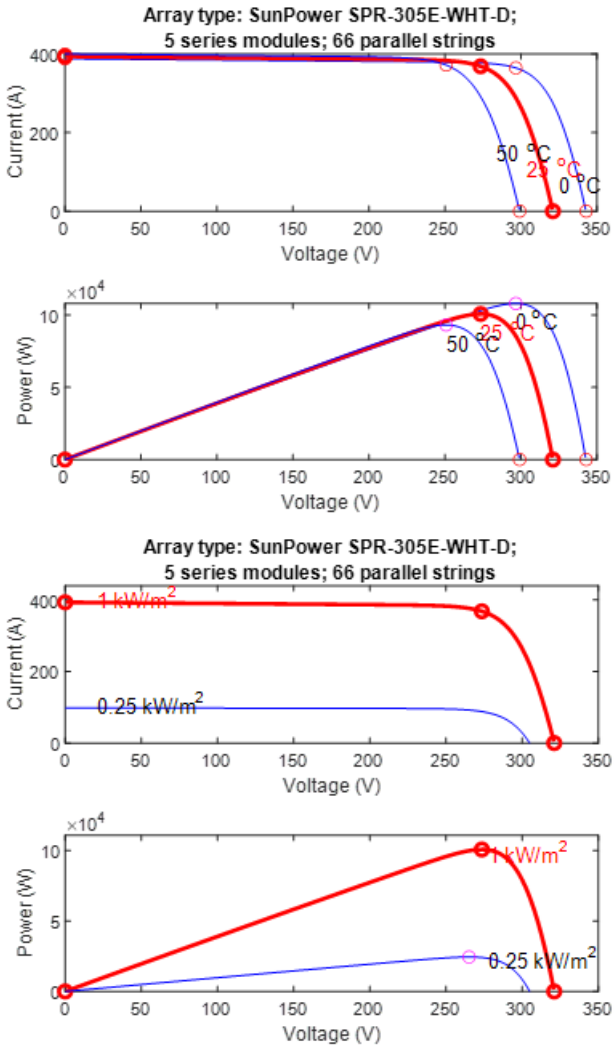


*Figure 12: lowest: I-V and P–V curves at various solar irradiations, above: I-V and P–V curves at various temperatures.*

Iterative algorithm code to find Rs and Rsh :

% Iterative algorithm to estimate Rs and Rsh (Rp) from datasheet parameters

%% 1. Datasheet parameters and nominal conditions

Iscn = 5.96;  % short-circuit current at STC [A]

Vocn = 64.2;  % open-circuit voltage at STC [V]

```
Imp  = 5.58;    % current at max-power point [A]

Vmp  = 54.7;    % voltage at max-power point [V]

Pmax_e = Vmp * Imp;  % datasheet peak power [W]

Kv = - 0.2727; % voltage temp-coeff [V/K]

Ki = 0.061745;    % current temp-coeff [A/K]

Ns = 96;        % number of cells in series

a  = 0.94489;       % diode ideality factor

Gn = 1000;              % irradiance at STC [W/m²]

Tn = 25 + 273.15;         % junction temperature at STC [K]


%% 2. Numerical-search settings

Rsinc  = 0.0001;    % how much to nudge Rs each outer iteration

tol    = 0.0001;    % acceptable power-error (W)

nv     = 5000;      % points on V axis for I–V curve

nimax  = 500000;    % max allowed iterations


%% 3. Initial guess for Rp and Rs

Rp_min = Vmp/(Iscn - Imp);  % a rough lower bound for Rp

Rs = 0;      % start with zero series resistance

Rp = Rp_min; % start here for shunt resistance


%% 4. Precompute constants

k  = 1.3806503e-23;    % Boltzmann's constant [J/K]
```

```
q  = 1.60217646e-19;   % elementary charge [C]
Vt = k * Tn / q;       % thermal voltage @ STC [V]

%% 5. Outer loop: match Pmax
perror = Inf;
ni     = 0;
T      = Tn;      % assuming STC temperature
dT     = T - Tn;  % zero for STC
G      = Gn;      % assuming STC irradiance

while (perror > tol) && (Rp > 0) && (ni < nimax)
  ni = ni + 1;

  % Compute equivalent light-generated current at Vmp
  Ipvn = (Rs + Rp)/Rp * Iscn;
  Ipv  = (Ipvn + Ki*dT) * G/Gn;
  Isc  = (Iscn + Ki*dT) * G/Gn;

  % Diode saturation current
  Io = (Iscn + Ki*dT) / (exp((Vocn + Kv*dT)/(Vt * a * Ns)) - 1);

  % Increment Rs
  Rs = Rs + Rsinc;
```

```
% Update Rp
Rp = Vmp*(Vmp + Imp*Rs)  ...
    /( Vmp*Ipv/Io*exp((Vmp + Imp*Rs)/(Vt*Ns*a)) ...
      + Vmp*Io - Pmax_e );

% Generate I–V curve and compute Pmax_m
V = linspace(0, Vocn, nv);
I = zeros(size(V));
for j = 1:length(V)
  g = @(Ival) Ipv - Io*(exp((V(j) + Ival*Rs)/(Vt*Ns*a)) - 1) - (V(j) + Ival*Rs)/Rp - Ival;
  dg = @(Ival) - Io*Rs/(Vt*Ns*a)*exp((V(j) + Ival*Rs)/(Vt*Ns*a)) - Rs/Rp - 1;
  Ival = 0;
  while abs(g(Ival)) > 1e-3
    Ival = Ival - g(Ival)/dg(Ival);
  end
  I(j) = Ival;
end
P = (Ipv - Io*(exp((V + I*Rs)/(Vt*Ns*a)) - 1) - (V + I*Rs)/Rp).*V;
Pmax_m = max(P);
perror = abs(Pmax_m - Pmax_e);
end
```

```
% Display results
disp('Model info:');
fprintf(' Rp = %f
', Rp);
fprintf(' Rs = %f
', Rs);
fprintf(' a = %f
', a);
fprintf(' T = %f
', T - 273.15);
fprintf(' G = %f
', G);
fprintf(' Pmax,m = %f (model)
', Pmax_m);
fprintf(' Pmax,e = %f (experimental)
', Pmax_e);
fprintf(' tol = %f
', tol);
fprintf(' P_error = %f
', perror);
fprintf(' Ipv = %f
', Ipv);
fprintf(' Isc = %f
```

', Isc);

fprintf(' Io = %g

', Io);

| | |
|---|---|
| $I_{mp}$ | 5.58 A |
| $V_{mp}$ | 54.7 V |
| $P_{max,e}$ | 305.226 W |
| $I_{sc,n}$ | 5.96 A |
| $V_{oc,n}$ | 64.2 V |
| $K_v$ | -0.2727V/K |
| $K_i$ | 0.061745 A/K |
| $N_s$ | 96 |

*Table 2 : Parameters of the SunPower SPR-305E-WHT-D PV module at 25 °C, 1000 W/m2*

| | |
|---|---|
| $I_{mp}$ | 5.58 A |
| $V_{mp}$ | 54.7 V |
| $P_{max,m}$ | 350.226 W |
| $I_0$ | $6.3076.10^{-12}$ A |
| $I_{PV}$ | 5.9657 A |
| a | 0.94489 |
| $R_s$ | 0.37428 Ω |
| $R_p$ | 393.2054Ω |

*Table 3 : The SunPower SPR-305E-WHT-D PV module's five parameters*

***III . 2 . 2 DC/DC converter and MPPT controller :***

The boost converter uses PWM technology, which is generated by the MPPT algorithm. The formula between Vpv and Vdc is given for continuous current conduction by Eq. (11) :

$$V_{dc} = \frac{V_{pv}}{(1-D)} \qquad (11)$$

The boost converter's inductance (L) is calculated by choosing an acceptable inductance current ripple that passes through it [26].

$$\Delta I_L = \frac{D.V_{pv}}{f_{sw-boost}.L} = \frac{D.(1-D).V_{dc}}{f_{sw-boost}.L}$$
$$\leftrightarrow L = \frac{D.V_{pv}}{f_{sw-boost}.\Delta I_L} \qquad (12)$$

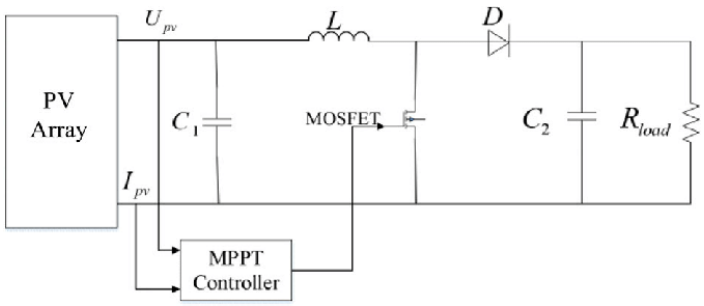


*Figure 13: Scheme of the boost converter in PV System.*

The duty cycle D is obtained by:

$$D = 1 - \frac{V_{pv}}{V_{dc}} \qquad (13)$$

Assuming no losses due to the resistive load R, Ppv is equal to Pdc.

$$R = \frac{V_{dc}^2}{P_{dc}} \qquad (14)$$

The Inductance current $I_L$ is given by:

$$P_{pv} = P_{dc} = \frac{V_{dc}^2}{R} \rightarrow I_L = \frac{V_{dc}^2}{R.V_{pv}} = \frac{V_{dc}}{R(1-D)} \qquad (15)$$

For the input capacitor $C_{pv}$, the relation is:

$$C_{pv} = \frac{D.V_{dc}}{Rf_{sw-boost}.\Delta V_{dc}} \qquad (16)$$

In order to avoid overvoltages and limit power oscillations, which have an impact on grid current, the DC-link capacitor should have the proper size. Equation (17) is used to select the value, taking into account 100% converter efficiency [26].

$$P_{ac} \approx P_{pv} \rightarrow C_{dc} = \frac{P_{ac}}{2.\omega.V_{dc}\Delta V_{dc}} \qquad (17)$$

The maximum power point (MPP) with optimal voltage and current is a unique point in the PV array I-V and P-V characteristics. Due to nonlinear I-V characteristics that vary with irradiation and temperature, the position of the MPP is unknown and it must be found. The perturb & observe

(P&O) and INC methods are the most often used MPPT methods. In this work, an MPPT controller is built using the INC algorithm depicted in Fig. 14. This technique is based on the observation that the slope of the P–V curve for a PV array is zero at its MPP, positive in the zone to the left of the MPP, and negative in the zone to the right of the MPP. The maximum output power is calculated by using Eq. (19) :

$$\frac{dP}{dV} = \frac{d(I.V)}{dV} = I + V\frac{dI}{dV} = I + V\frac{\Delta I}{\Delta V} \qquad (18)$$

$$\frac{dP}{dV} = 0 \leftrightarrow \frac{\Delta I}{\Delta V} = -\frac{I}{V} \text{at MPP} \qquad (19)$$

$$\frac{dP}{dV} > 0 \leftrightarrow \frac{\Delta I}{\Delta V} > -\frac{I}{V} \text{left of MPP} \qquad (20)$$

$$\frac{dP}{dV} < 0 \leftrightarrow \frac{\Delta I}{\Delta V} < -\frac{I}{V} \text{right of MPP} \qquad (21)$$

To track the MPP, the instantaneous conductance and incremental conductance are compared. The PV module's operation remains at the MPP unless a change in current due to varying meteorological parameters alters the MPP.

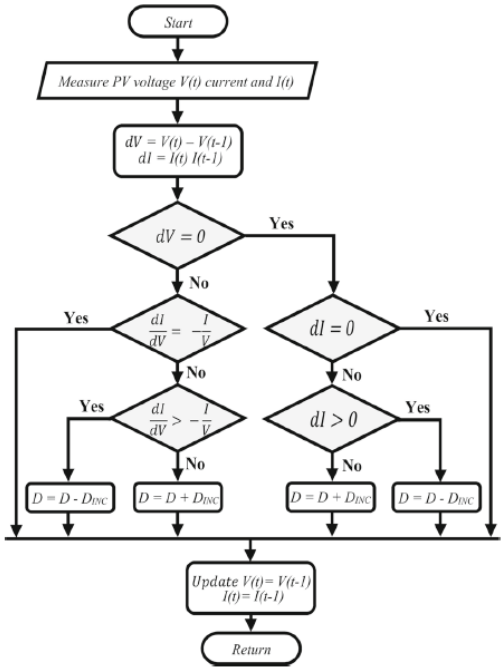


*Figure 14: Flowchart of INC algorithm.*

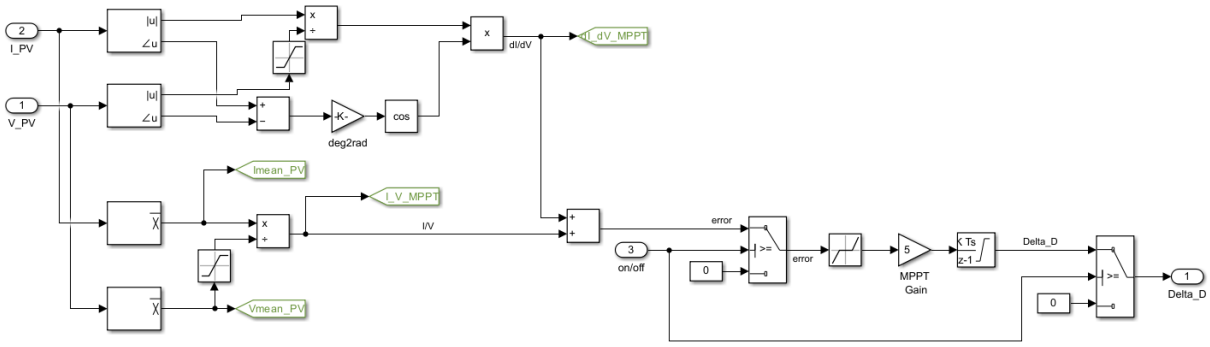


```
Maximum power point tracking by incremental conductance method
-------------------------------------------------------------
Maximum power point is obtained when dP/dV=0  where P= V*I
-> d(V*I)/dV = I + V*dI/dV = 0
-> dI/dV = -I/V

dI, dV  = fundamental components of I and V ripples measured with a sliding time window T_MPPT
I , V   = mean values of V and I measured with a sliding time window T_MPPT

The integral regulator minimizes the error (dI/dV + I/V)
Regulator output = Duty cycle correction
```

*Figure 15: INC-based MPPT controller in Simulink.*

### *III. 3 Modeling and control of AC stage :*

### *III . 3 . 1 Selection of DC-Link:*

Based on the criteria mentioned in [27], Vdc for VSI should be 10-15% more than the voltage of the charged capacitor, as it is crucial for controlling the three-phase output voltage of the PWM inverter. Also, it should be noted that regulation of current flow is only possible if Vdc is above the sum of the peak grid voltage and the drop between the grid and the inverter.

If the phase root mean square (RMS) grid voltage of the present work is 150 V, then the uncontrolled VSI output voltage is 260 V. For systems using sinusoidal pulse width modulation (SPWM) VSI, a 15% criterion is applied, and Vdc = 500 V is selected as the reference dc-link voltage. The line-to-line voltage VLL is obtained using Eq. (22), where $m_a$ is the modulation index:

$$V_{LL} = \frac{\sqrt{3}.V_{dc}.m_a}{2.\sqrt{2}} \text{(SPWM)} \quad (22)$$

A DC-link voltage of 500 V is chosen for the studied system, as per Eq. (22).

### *III . 3 . 2 DC/AC converter:*

According to the classification of industrial inverter topologies given by [28], central inverters can be three-level T-type (3L-T-type), three-level neutral point clamped (3L-NPC), or two-level voltage source inverters (2L-VSI).

#### *III . 3 .2 .1 Modeling of SPWM 3L-VSI:*

The boost converter's 500 V DC output voltage is converted in this work to 260 V AC at a frequency of 60 Hz using a 3L-VSI.

The SPWM technique is chosen for its simplicity to produce the IGBT's gate signals. This method allows the regulation of three-phase output voltages, amplitude, and frequency. a high-frequency carrier signal in a triangular waveform with a 1980 Hz frequency is compared to three reference or modulating signals in a sinusoidal waveform, each assigned to a different phase,

separated by a phase shift of 120°. The results of the comparison are used to properly activate the switches on each leg. In the investigated system, reference signals are obtained from the inverter controllers (outer and inner loops).

### *III . 3 . 3 LC filter design:*

The LC filter is chosen for the studied system since it is commonly used with VSI in grid-connected PV systems due to its advantages over other filter topologies. Despite this, filter is unstable due to resonance and may result in input current distortion in both dynamic and steady-state [29]. To solve this, passive damping is utilized, which involves connecting a damping resistor either in series or parallel with the filter capacitor or the inductance on the inverter side[30] . To design an LC filter for the studied system a Matlab program was developed to implement the algorithm shown in Fig. 16. Two conditons must be met: resonance frequency within Eq. (32) range and total filter inductance smaller than 0.1 per unit (pu) to reduce AC voltage drop. the LC filter's transfer function is given by:

$$Y_{LC} = \frac{I_g(S)}{V_i(S)} = \frac{S.C_f.R_d+1}{S^2.C_f.L_i+SC_fR_d} \qquad (23)$$

Two conditons must be met: resonance frequency within Eq. (32) range and total filter inductance smaller than 0.1 per unit (pu) to reduce AC voltage drop.

$$C_f = x.C_b \qquad (24)$$

$$C_b = \frac{1}{2\pi f_g Z_b} \qquad (25)$$

$$V_{LL,rms} = \sqrt{3}V_{ph} \qquad (26)$$

$$Z_b = \frac{V_{LL,rms}^2}{P_{rated}} \qquad (27)$$

$$L_i = \frac{V_{dc}}{8.f_{sw-vsi.(15\%I_b)}} \quad (28)$$

$$I_b = \frac{P_{rated}}{\sqrt{3}V_{LLrms}} \quad (29)$$

$$f_{res} = \frac{1}{2\pi}\sqrt{L_i C_f} \quad (30)$$

$$R_d = \frac{1}{3(2\pi f_{res} C_f)} \quad (31)$$

$$10.f_g < f_{res} < \frac{f_{sw-vsi}}{2} \quad (32)$$

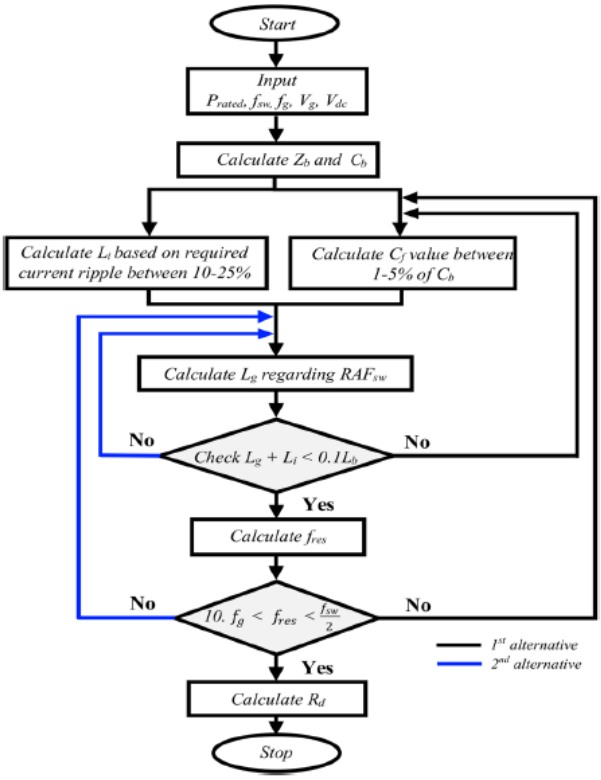


*Figure 16: LC filter design flowchart .*

### *III . 3 . 4 Phase locked loop (PLL) :*

For the grid-connected VSI, grid synchronization must fulfill the grid code requirements. Therefore, the PLL plays a crucial role in determining the phase angle θg, as well as the voltage components in the dq frame at the PCC. For an ideal balanced three-phase grid, the synchronous

reference frame phase-locked loop (SRF-PLL) follows a simple process. Initially, both the Clarke and Park transformations are applied. The mean of the PI controller sets the reference quantity Vq* to zero [31] . The angular frequency ω, expressed in rad/s, is provided by the PI controller. This term's integration yields the phase angle θ, expressed in radians. The angle is correctly wrapped by the modulo block, which also keeps it between 0 and 2π. For a balanced three-phase grid with a 120-degree phase shift:

$$\begin{cases} V_a = V_m \sin(\theta) \\ V_b = V_m \sin(\theta - \frac{2\pi}{3}) \\ V_c = V_m \sin(\theta + \frac{2\pi}{3}) \end{cases} \quad (33)$$

Here, $V_m$ represents the amplitude of phase voltage, and θ denotes the voltage phase. Following the use of Clarke transformation matrix C:

$$[V_\alpha V_\beta] = \mathrm{C}[V_a V_b V_c]^T \quad (34)$$

$$\mathbf{C} = \frac{2}{3}\begin{bmatrix} 1 & \frac{-1}{2} & \frac{-1}{2} \\ 0 & \frac{\sqrt{3}}{2} & \frac{-\sqrt{3}}{2} \end{bmatrix} \quad (35)$$

$$\begin{cases} V_\alpha = V_m \sin\theta \\ V_\beta = -V_m \cos\theta \end{cases} \quad (36)$$

Implementing the Park transformation matrix P and assuming that the PLL error, θ–θ', is negligible:

$$[x_d x_q] = \mathbb{P}[x_\alpha x_\beta]^T \quad (37)$$

$$P = \begin{bmatrix} cos\theta' sin\theta' \\ -sin\theta' cos\theta' \end{bmatrix} \quad (38)$$

$$\begin{cases} V_d = V_\alpha \cos\theta' + V_\beta \sin\theta' \approx V_m \\ V_q = -V_\alpha \sin\theta' + V_\beta \cos\theta' \approx -V_m(\theta - \theta') \end{cases} \quad (39)$$

The approximation $\sin(\Delta\theta) \approx \Delta\theta$ if $\Delta\theta \to 0$, The open loop transfer function:

$$G_{OL-PLL}(s) = \frac{K_{p-pll}S + K_{i-pll}}{S^2}(-V_m) \quad (40)$$

The closed-loop transfer function :

$$G_{CL-PLL}(s) = \frac{-V_m(K_{p-pll}S+K_{i-pll})}{S^2-V_m.K_{p-pll}S-V_m.K_{i-pll}} \qquad (41)$$

By identifying the denominator of Eq. (41) with that of the standard form of second order systems, Eq. (42), the PI controller gains are determined.

$$S^2 + 2\xi\omega_n S + \omega_n^2 \qquad (42)$$

$$\begin{cases} K_{p-pll} = \frac{-2\xi\omega_n}{V_m} \\ K_{i-pll} = \frac{-\omega_n^2}{V_m} \end{cases} \qquad (43)$$

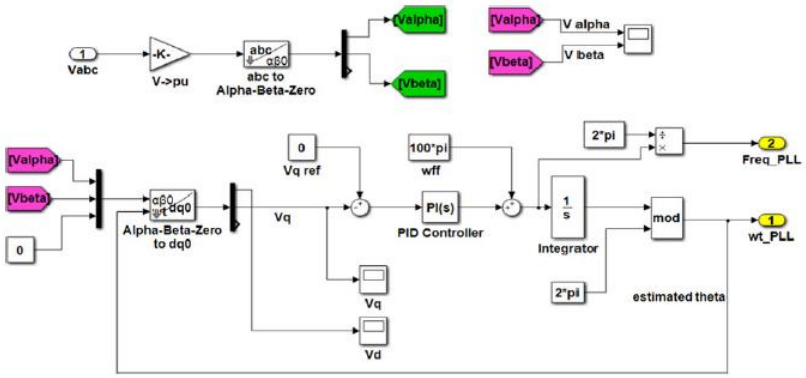


*Figure 17 : Simulink model for the SRF-PLL.*

### *III . 3 . 5 VSI controller design :*

To keep a constant voltage at the DC-link, the outer loop must generate Id* for the inner loop while regulating the active current injected into the VSI. It is crucial to note that the outer loop works on obtaining appropriate regulation and stability, while the inner loop aims for short settling times and unity gain. Consequently, effective decoupling of these loops is achieved by designing the outer loop to be 5–20 times slower, as suggested in [32] .

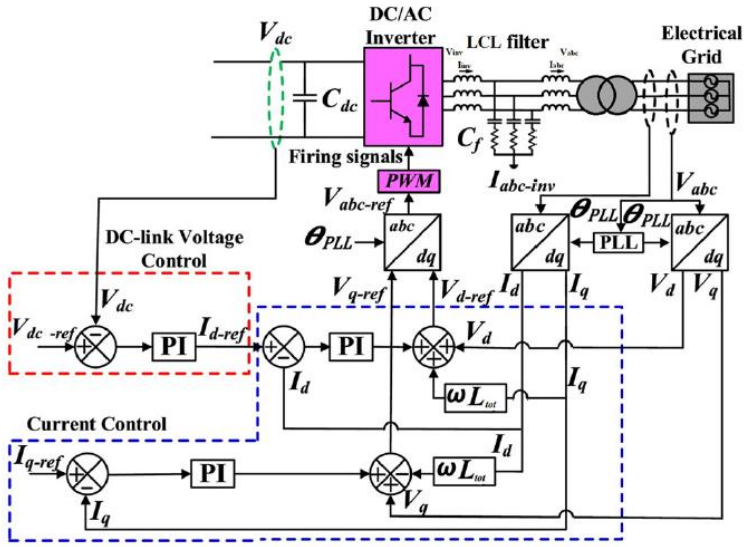


*Figure 18 : Diagram of VSI controller with grid side current feedback.*

### *III . 3 .5 .1 Inner loop design :*

In the grid side current feedback (GSCF) configuration, the filter capacitor is not considered. Thereby, to ensure a zero phase shift between the current and voltage of the grid (i.e., unity power factor) [30], the refer- ence current Iq* is set to zero. The time derivatives of the VSI output current are given by:

$$L_{tot}\frac{dI_{abc}}{dt} = V_{inv} - V_{abc} \quad (44)$$

where $V_{inv}$ is the inverter voltage, $I_{abc}$ and $V_{abc}$ are the grid current and voltage, respectively, and $L_{tot}$ is the total filter's inductance.

Through multiplication of both sides of Eq. (44) with the Clarke-Park transformation, the VSI is modeled in the dq frame with Eq. (46) :

$$T = \sqrt{\frac{2}{3}}\begin{bmatrix} \cos(\omega t) & \cos\left(\omega t - \frac{2\pi}{3}\right) & \cos\left(\omega t + \frac{2\pi}{3}\right) \\ -\sin(\omega t) & -\sin\left(\omega t - \frac{2\pi}{3}\right) & -\sin\left(\omega t + \frac{2\pi}{3}\right) \\ \frac{1}{\sqrt{2}} & \frac{1}{\sqrt{2}} & \frac{1}{\sqrt{2}} \end{bmatrix} \quad (45)$$

$$\begin{bmatrix} V_{inv,d} \\ V_{inv,q} \end{bmatrix} = L_{tot}\frac{d}{dt}\begin{bmatrix} I_d \\ I_q \end{bmatrix} + L_{tot}\begin{bmatrix} 0 & -\omega \\ \omega & 0 \end{bmatrix}\begin{bmatrix} I_d \\ I_q \end{bmatrix} + \begin{bmatrix} V_d \\ V_q \end{bmatrix} \quad (46)$$

To compensate for the cross-coupling term in Eq. (46), decoupling terms $+\omega L_{tot}I_q$ and $-\omega L_{tot}I_d$ are included in the outputs of the PI controllers for the d and q axes, respectively.

At the inverter output, the following control rules generate the reference voltages:

$$V_{inv,d}^{*} = \left(K_{p-c} + \frac{K_{i-c}}{s}\right)(I_d^{*} - I_d) + L_{tot}\omega I_q + V_d \quad (47)$$

$$V_{inv,q}^{*} = \left(K_{p-c} + \frac{K_{i-c}}{s}\right)(I_q^{*} - I_q) - L_{tot}\omega I_d + V_q \quad (48)$$

In order to provide the switching signals for the VSI, $V_{inv,d}^{*}$ and $V_{inv,q}^{*}$ are initially converted back into the abc frame.

the PI controller's gains are adjusted as follows:

$$\begin{cases} K_{p-c} = \frac{L_i + L_g}{\alpha T_{inner}} \\ T_{i-c} = \alpha^2 T_{inner} \end{cases} \quad (49)$$

$$\alpha = 2\xi + 1 \quad (50)$$

the inner loop time $T_{inner}$ is equal to $\alpha^2 T_{eq}$, and the parameter α is selected as in Eq. (50) to achieve the desirable damping ξ.

There are some delays in the control loop that must be included in the control scheme modeling, namely the digital processing delay and the PWM transport delay . It has commonly been modeled as a combination of one sample time delay $T_{s-c}$ as a processing delay and a delay of $0.5T_{s-c}$ caused by a zero-order hold of the digital PWM. Thus, the equivalent delay time constant of this loop corresponds to $T_{eq}=1.5T_{s-c}$, where $T_{s-c}$ corresponds to the sample time for the inner control loop. Additionally, the LC filter is reduced to a first-order delay element since the dq axes are decoupled, which improves the PI controllers' tracking capabilities [33].

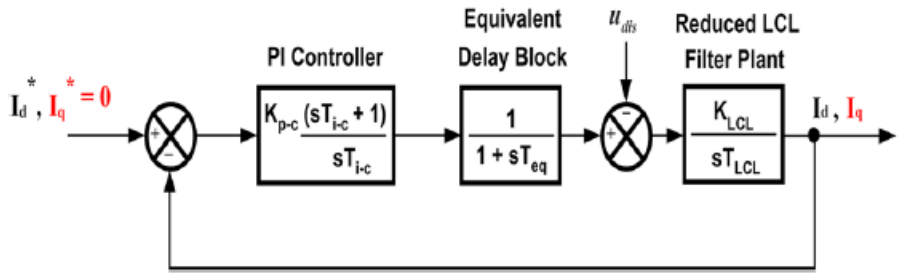


*Figure 19 : Inner current control loop.*

### *III . 3 .5 .2 Outer loop design :*

Assuming no losses on the VSI and applying the power balance between $P_{ac}$ and $P_{dc}$ :

$$P_{dc} \approx P_{ac} \rightarrow v_{dc} i_{dc} - v_{dc} C_{dc} \frac{dv_{dc}}{dt} = \frac{3}{2}(v_d i_d + v_q i_q) \quad (51)$$

For the study of the outer loop, an equivalent first-order transfer function is applied to approximate the GSCF controller closed-loop. the PI controller gains are determined according to SO criterion.

$$v_{dc}(s) = \frac{1}{sC_{dc}}\left(i_{dc}(s) - \frac{3}{2}\frac{V_m}{v_{dc}} i_d(s)\right) \quad (52)$$

$$I_d^* = (K_{p-v} + \frac{K_{i-v}}{s})(V_{dc}^* - V_{dc}) \quad (53)$$

$$\begin{cases} K_{p-v} = -\frac{2V_{dc}C_{dc}}{3V_m \alpha T_{outer}} \\ T_{i-v} = \alpha^2 T_{outer} \end{cases} \quad (54)$$

where the outer loop time $T_{outer}$ is the sum of the sample time for the dc-link voltage control loop $T_{s-v}$ and $T_{inner}$.

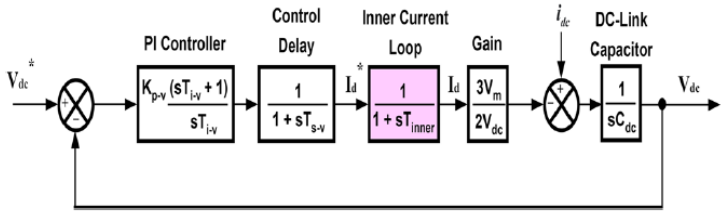


*Figure 20 : Control loop of dc-link voltage.*

# Chapter IV : Results and Discussion

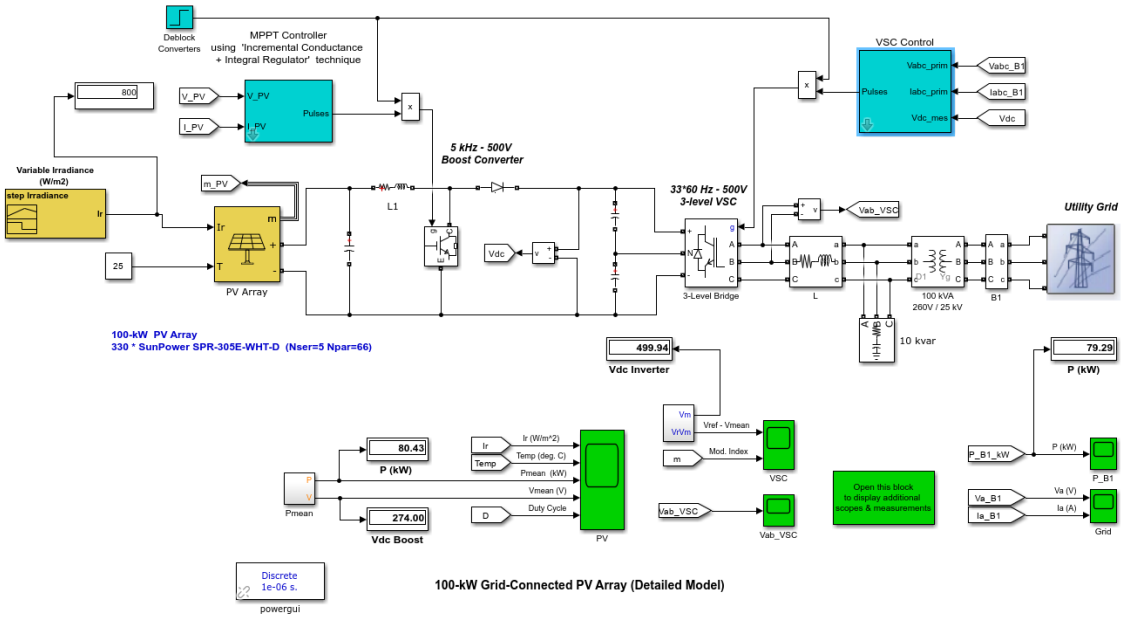


*Figure 22: Simulink model of 100 kW PV plant.*

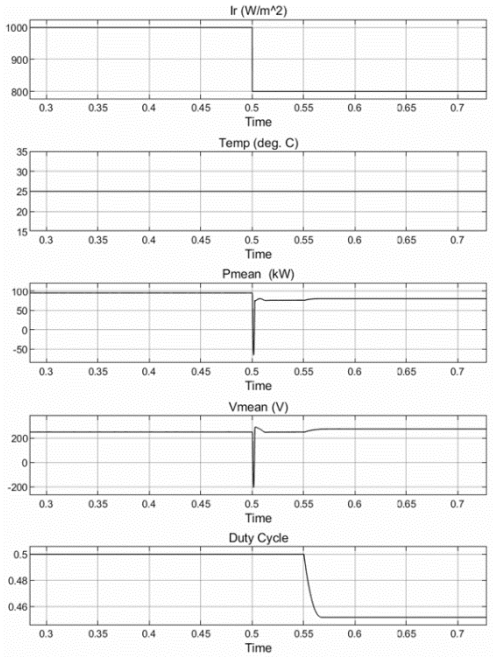


*Figure 21: a Solar irradiance and temperature profile, b PV array output power, c PV array output voltage, d duty cycle of MPPT controller*

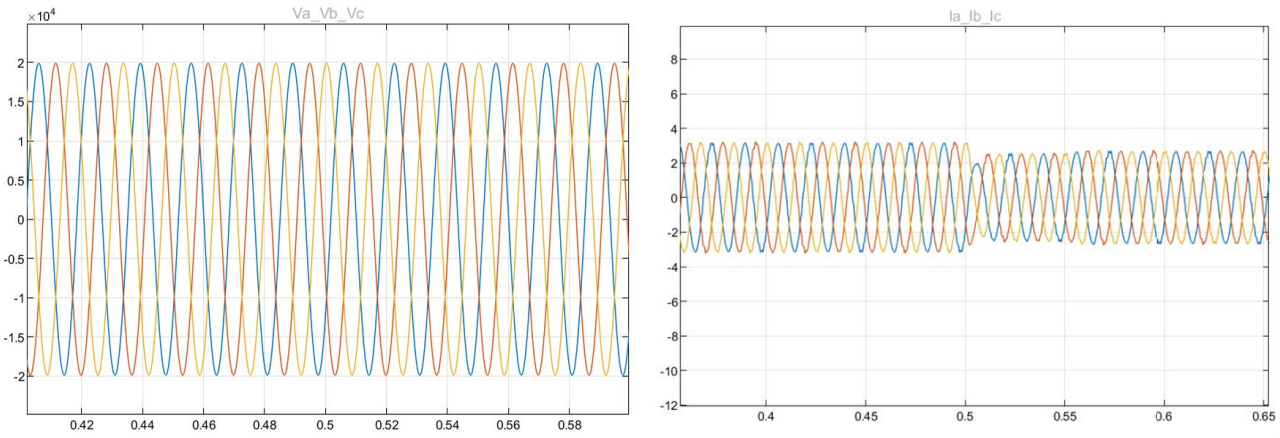


*Figure 23: Grid voltage and grid current waveforms at PCC.*

The simulation is conducted under STC (G 1000 W/m² and T 25°C). Then, to evaluate the dynamic and steady-state behavior of the PV array's control system, a sudden fall in solar irradiation is performed at 0.5 s. This circumstance may arise when a cloud blocks the PV array from receiving direct sunlight as it passes over-head. To do so, the DC and AC outputs and the associated PCU were monitored during this unexpected decrease in solar irradiation from 1000 to 800 W/m². The temperature was set to be constant at 25°C for all simulations. after 2 ms, the PV generator delivers its optimum current, which is 350 A with a voltage of approximately 300 V, and generates a power of 100 kW, which corresponds to the power at MPP. Both Ipv and Ppv were more affected by the drop in solar irradiation than Vpv, where the effect on the latter was very small. They decreased from 350 to 300 A and from 100 to 80.43 kW, with a reduction rate of 20%. This was expected since the Ipv is confirmed to be proportional to solar irradiation. we can see that the grid's voltage and current waveforms at PCC reached steady-state after just 3 AC cycles, and its performance under STC was very good. However, the sudden decrease in irradiance at t

0.5 s causes a reduction in the grid current amplitude, but it does not affect the dynamic behavior of the grid voltage waveform at PCC since it is determined by the AC network.

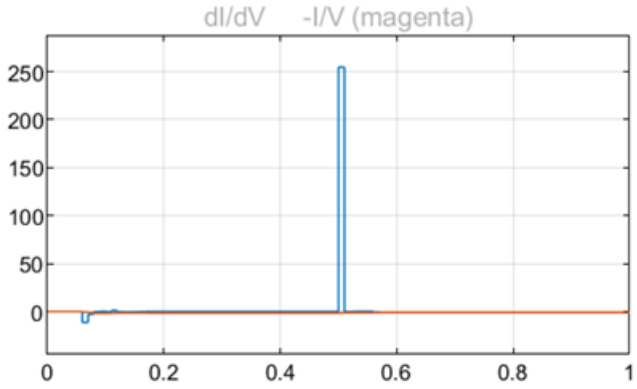


*Figure 24 : MPPT algorithm results.*

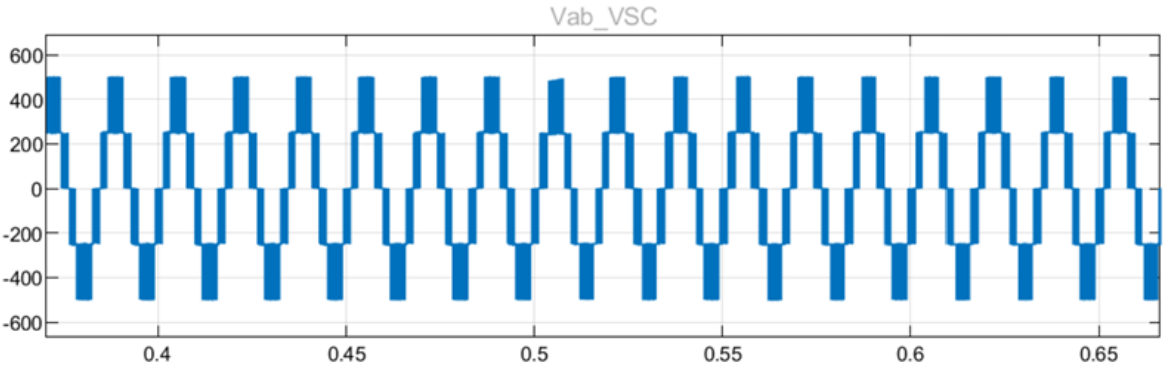


*Figure 25: Simulated line-to-line voltages for 3L-VSI_Vab.*

## Chapter V : Conclusion

The detailed model and control strategy of a 100 kW grid connected PV system, are presented in this thesis. Then, the final model of the whole system is simulated inMatlab/Simulink under different weather conditions, namely standard test conditions (STC), a sudden drop in solar irradiation. Simulation results consistently demonstrated compliance with technical requirements for PV system interconnection to the grid recommended by IEEE and EN. Under constant irradiance, the system achieved a low current harmonic distortion (THD) of less than 5%, maintained the frequency at the PCC within the 60 Hz , and ensured unity power factor through effective grid synchronization. Even when subjected to a sudden drop in sunlight irradiance, the dynamic response of the PV control system was robust, and both the incremental conductance (INC)-based MPPT and the voltage source inverter (VSI) controllers were able to track and adapt to the change in power level while remaining within the recommended standard ranges.

In conclusion, this research contributes to the advancement of grid-connected PV systems by offering a robust modeling and control framework. Future work may explore hardware-in-the-loop (HIL) validation, fault ride-through capabilities, and the integration of energy storage systems to further enhance system flexibility and resilience.

## References


[1] D. P. Cassidy and R. L. Irvine, “The effect of operating conditions on the performance of soil slurry-SBRs,” *Water Sci. Technol.*, vol. 43, no. 3, pp. 223–230, 2001, doi: 10.2166/wst.2001.0141.

[2] E. Martinot, “Renewables global futures report,” *Paris Renew. Energy Policy Netw.*, 2013.

[3] W. Omran, “Performance Analysis of Grid-Connected Photovoltaic Systems,” pp. 1–196, 2010.

[4] A. Al-Salaymeh, Z. Al-Hamamre, F. Sharaf, and M. R. Abdelkader, “Technical and economical assessment of the utilization of photovoltaic systems in residential buildings: The case of Jordan,” *Energy Convers. Manag.*, vol. 51, no. 8, pp. 1719–1726, 2010, doi: 10.1016/j.enconman.2009.11.026.

[5] A. Loukriz, S. Messalti, and A. Harrag, “Design, simulation, and hardware implementation of novel optimum operating point tracker of PV system using adaptive step size,” *Int. J. Adv. Manuf. Technol.*, vol. 101, no. 5–8, pp. 1671–1680, 2019, doi: 10.1007/s00170-018-2977-7.

[6] P. E. Posedly, “Modeling and Analysis of Photovoltaic Generation and Storage Systems for Residential Use Master of Science,” *Electr. Eng.*, pp. 1–105, 2008.

[7] V. Lo Brano, A. Orioli, G. Ciulla, and A. Di Gangi, “An improved five-parameter model for photovoltaic modules,” *Sol. Energy Mater. Sol. Cells*, vol. 94, no. 8, pp. 1358–1370, 2010, doi: 10.1016/j.solmat.2010.04.003.

[8] R. Baños, F. Manzano-Agugliaro, F. G. Montoya, C. Gil, A. Alcayde, and J. Gómez, “Optimization methods applied to renewable and sustainable energy: A review,” *Renew.*

*Sustain. Energy Rev.*, vol. 15, no. 4, pp. 1753–1766, 2011, doi: 10.1016/j.rser.2010.12.008.

[9] J. Assadeg, K. Sopian, and A. Fudholi, "Performance of grid-connected solar photovoltaic power plants in the Middle East and North Africa," vol. 9, no. 5, pp. 3375–3383, 2019, doi: 10.11591/ijece.v9i5.pp3375-3383.

[10] J. Hossain and A. Mahmud, *Renewable energy integration: challenges and solutions*. Springer Science & Business Media, 2014.

[11] D. G. F. Sonnenenergie, *Planning and installing photovoltaic systems: a guide for installers, architects and engineers*. Earthscan, 2007.

[12] R. A. Messenger, *Photovoltaic systems engineering*. CRC press, 2018.

[13] S. B. Kjaer, J. K. Pedersen, and F. Blaabjerg, "A review of single-phase grid-connected inverters for photovoltaic modules," *IEEE Trans. Ind. Appl.*, vol. 41, no. 5, pp. 1292–1306, 2005.

[14] B. M. T. Ho, S.-H. Chung, and S. Y. R. Hui, "An integrated inverter with maximum power tracking for grid-connected PV systems," in *Nineteenth Annual IEEE Applied Power Electronics Conference and Exposition, 2004. APEC'04.*, IEEE, 2004, pp. 1559–1565.

[15] I.-S. Kim, M.-B. Kim, and M.-J. Youn, "New maximum power point tracker using sliding-mode observer for estimation of solar array current in the grid-connected photovoltaic system," *IEEE Trans. Ind. Electron.*, vol. 53, no. 4, pp. 1027–1035, 2006.

[16] S. Liu, J. Liu, S. Member, H. Mao, and Y. Zhang, "Analysis of Operating Modes and Output Voltage Ripple of Boost DC – DC Converters and Its Design Considerations," vol. 23, no. 4, pp. 1813–1821, 2008.

[17] N. Femia, G. Petrone, G. Spagnuolo, and M. Vitelli, "A technique for improving P&O MPPT performances of double-stage grid-connected photovoltaic systems," *IEEE Trans.*

*Ind. Electron.*, vol. 56, no. 11, pp. 4473–4482, 2009.

[18] A. Abo-Khalil *et al.*, "Comparison Among Different Maximum Power Point Tracking Techniques of Solar Photovoltaic Systems," *Hussein Mohamed Wilberforce, Tabbi Olabi, Abdul Ghani, Comp. Among Differ. Maximum Power Point Track. Tech. Sol. Photovolt. Syst.*.

[19] J. K. Steinke, "Use of an LC filter to achieve a motor-friendly performance of the PWM voltage source inverter," *IEEE Trans. Energy Convers.*, vol. 14, no. 3, pp. 649–654, 2002.

[20] G. H. P. Ooi, "Investigation and implementation of multilevel power converters for low/medium/high power applications," 2015.

[21] A. Nabae, I. Takahashi, and H. Akagi, "A new neutral-point-clamped PWM inverter," *IEEE Trans. Ind. Appl.*, no. 5, pp. 518–523, 1981.

[22] I. Colak, E. Kabalci, and R. Bayindir, "Review of multilevel voltage source inverter topologies and control schemes," *Energy Convers. Manag.*, vol. 52, no. 2, pp. 1114–1128, 2011.

[23] K. Bouchouicha, N. Bailek, A. Razagui, M. EL-Shimy, M. Bellaoui, and N. E. I. Bachari, "Comparison of artificial intelligence and empirical models for energy production estimation of 20 MWp solar photovoltaic plant at the Saharan Medium of Algeria," *Int. J. Energy Sect. Manag.*, vol. 15, no. 1, pp. 119–138, 2021.

[24] M. G. Villalva, J. R. Gazoli, and E. Ruppert Filho, "Modeling and circuit-based simulation of photovoltaic arrays," in *2009 Brazilian power electronics conference*, IEEE, 2009, pp. 1244–1254.

[25] C. Series, "CELL SERIES," 2008.

[26] N. E. Zakzouk, A. K. Abdelsalam, A. A. Helal, and B. W. Williams, "PV single-phase grid-

connected converter: DC-link voltage sensorless prospective," *IEEE J. Emerg. Sel. Top. Power Electron.*, vol. 5, no. 1, pp. 526–546, 2016.

[27] T. R. Nath, "Solar Photovoltaic Power Generating System & Grid Integration-Modeling, Controller Design and Optimization," 2017.

[28] K. Zeb *et al.*, "An overview of transformerless inverters for grid connected photovoltaic system," in *2018 International Conference on Computing, Electronic and Electrical Engineering (ICE Cube)*, IEEE, 2018, pp. 1–6.

[29] H. B. Massawe, "Grid connected photovoltaic systems with smartgrid functionality," 2013, *Institutt for elkraftteknikk*.

[30] E. Kantar, "Design and control of PWM converter with LCL type filter for grid interface of renewable energy systems," 2014, *Middle East Technical University (Turkey)*.

[31] N. Mennai, Y. Soufi, A. Medoued, and A. Faleh, "Grid synchronization techniques analysis of DG systems under grid fault conditions," in *2022 19th International Multi-Conference on Systems, Signals & Devices (SSD)*, IEEE, 2022, pp. 917–922.

[32] S. M. Tripathi, A. N. Tiwari, and D. Singh, "Optimum design of proportional-integral controllers in grid-integrated PMSG-based wind energy conversion system," *Int. Trans. Electr. Energy Syst.*, vol. 26, no. 5, pp. 1006–1031, 2016.

[33] G. Elhassan, S. A. Zulkifli, E. Pathan, M. H. Khan, and R. Jackson, "A comprehensive review on time-delay compensation techniques for grid-connected inverters," *IET Renew. Power Gener.*, vol. 15, no. 2, pp. 251–266, 2021.